buildings

MDPI

Article

Permeability Prediction Model Modified on Kozeny-Carman for Building Foundation of Clay Soil

Jian Chen [1], Huawei Tong [1], Jie Yuan [1,*], Yingguang Fang [2] and Renguo Gu [2]

[1] School of Civil Engineering, Guangzhou University, Guangzhou 510006, China
[2] School of Civil Engineering & Transportation, South China University of Technology, Guangzhou 510641, China
* Correspondence: jiey8904@163.com; Tel.: +86-18565519891

Abstract: Clay soil is a common building foundation material, and its permeability is very important for the safety of foundation pits and the later settlement of buildings. However, the traditional Kozeny-Carman (K-C) equation shows serious discrepancies when predicting the permeability of clay in building foundation treatment. Therefore, solving the application of K-C equation in clay is a problem faced by the engineers and scholars. In this paper, the influence of clay mineralogy on pore structure and permeability is analyzed, and then the effective e (e_{eff}) and effective SSA (S_{eff}) are proposed. Based on the e_{eff} and S_{eff}, the permeability prediction model modified on Kozeny-Carman is built. Then, seepage experiments are conducted on two types of clay samples to test this prediction model; at the same time, the MIP combining freeze-drying methods are used to obtain the S_{eff} and e_{eff}. Through the discussion of the test results, three main conclusions are obtained: (1) there are invalid pores in clay due to the influence of clay mineral, this is the reason for which K-C equation is unsuitable for clay; (2) the e_{eff} and S_{eff} can reflect the structural state of clay during seepage; (3) the results of the permeability prediction model in this paper agree well with the test results, which indicates that this prediction model is applicable to clay. The research results of this paper are significant to solve the academic problem that K-C equation is not applicable to clay and significant to ensure the safety of building foundation pits in clay areas.

Keywords: building foundation; permeability of clay; clay mineral; K-C equation; pore connectivity; specific surface area

Citation: Chen, J.; Tong, H.; Yuan, J.; Fang, Y.; Gu, R. Permeability Prediction Model Modified on Kozeny-Carman for Building Foundation of Clay Soil. *Buildings* **2022**, *12*, 1798. https://doi.org/10.3390/buildings12111798

Academic Editors: Yue-Ling Long, Zhenhao Zhang, Ying Qin, Zhiliang Zuo and JinJing Liao

Received: 16 September 2022
Accepted: 17 October 2022
Published: 27 October 2022

1. Introduction

Soil is the most basic foundation material for buildings. The engineering properties of the soil are directly related to the safety of the buildings. For example, the mechanics and permeability properties of the soil are directly related to the groundwater treatment and the supports arrangement of the building foundation pit [1–3]. The later settlement of the foundation caused by the secondary consolidation of the soil directly affects the safe use of the buildings [4–6], for example, the leaning Bisha Tower is a typical representative. The solutions to the above problems are all directly linked to hydraulic conductivity of the soil, which is an important parameter to the permeability of soil. Unfortunately, the hydraulic conductivity is a difficult parameter to determine because it is closely related to soil structures, porosity, bulk density, saturation and fluid type [7,8]. Therefore, scholars have proposed many permeability calculation methods and prediction models [7,9–23].However, the most widely used are still Darcy's law and the K-C equation.

The K-C equation is very popular in the geotechnical engineering due to its fewer parameters. The K-C equation accounts well for the dependency of permeability on void ratio (e) in uniformly graded sands and some silts, however, serious discrepancies are often found when it is applied to clays [7].

In theory, hydraulic conductivity mainly depends on the pore size and the pores distribution [8]. Therefore, pore structure, e, SSA, tortuosity, and shape of the flow channels,

are always the hot points to explore the applicability of the K-C equation in clay. Except the pore tortuousness and pore shape [24–32], scholars have paid more attention to the e and the SSA of clay, and proposed various correction methods.

(1) void ratio (e)

The e is the standard of the amount of the flow channels, which is the decisive factor of the soil permeability. Therefore, the use of e in the K-C equation firstly aroused the attention. In fact, some pores are unconnected in clay and the water inside is not free to move. So, Taylor [20] suggested that the equation should be corrected by effective e, which was the ratio of free water volume to the particles. Later, more and more scholars expressed the similar views [33–35]. However, the test results reported by Mesri and Olson [19] showed that the hydraulic conductivity was higher for montmorillonite in nonpolar fluids than in water. At the same time, Horton et al. [36] found that the soil with different chemical solutions had different hydraulic conductivity. For the above phenomena, Meegoda et al. [37] proposed that except for the unconnected pores, the water held onto the particles by the electrolytic system forces also should be considered, because this part of water showed an elastic behavior and a solid-like structure rather than fluid [38]. In this case, Ren et al. [7] thought the void containing immobile water had no contribution to flow. At the same time, Dolinar and Trcek [39] thought that the water adsorbed onto surfaces of the clay mineral was immobile.

Therefore, the effective void should be the volume of total void minus the volume of unconnected pores and immobile water. But how to determine the volume of unconnected pores, immobile water and total void accurately is a tricky problem. In1984, one EPA determined the e_{eff} using the mercury intrusion porosimeter (MIP), this method could determine the invalid pores [36]. Meegoda et al. [37] proposed a method by chemical tracer tests to measure the effective void. Koponen et al. [40] used the lattice-gas method and simulated the effective e as a function of e. Meanwhile, Singh and Wallender [41] gave the effective e considering the thickness of the adsorbed water layer and the SSA of the clay. Urumović [42] presented the effective e in the function of referential grain size based on literature data. After reviewing the definitions and calculation methods by many scholars, Dolinar and Trcek [39] emphasized that effective e depended mostly on the external SSA of the soils. Wang et al. [10] considered the influence of bound water, and established a relationship between the effective e and the total e.

(2) SSA

For sandy soil, particle size is big and the geometric shape is regular, so the SSA proposed in the early days was mostly based on the geometric shape and size distribution curve of the particles [16,43–46]. For clay, the particle size is small and the shape parameter is difficult to determine, therefore, the method for sand soil is not suitable for clay. Of course, there are many ways to determine the SSA of clay, such as Methylene blue (MB) [47,48], Ethylene glycol monomethyl ether (EGME) [49,50] and Brunauer, Emmett and Teller method (BET) [47,51], several of them requiring high-tech equipment, so they are not commonly used. Therefore, some parameters of clay, such as Atterberg limits, liquid limit (LL) and soil water characteristic curve (SWCC), are used to establish empirical formulas with the SSA [52,53]. For example, Jacques Locat [54] proposed a correlation between Atterberg limits and SSA. Cerato [55] listed 12 correlations between the LL and SSA and then built a relationship between LL and SSA. Macek et al. [56] used 90 samples to estimate the relationship between the SWCC with the SSA. Kobayashi et al. [57] used X-ray diffraction to measure the SSA of compacted bentonite under constant volume conditions. In addition, Ismeik [58] presented artificial neural network models to estimate the SSA. Sharma [59] proposed a multivariate probabilistic approach for estimation of cation exchange capacity and SSA. Meegoda [60] proposed a method based on the electrical properties of soils in situ SSA. However, Dolinar [61,62] repeated that when using the LL to calculate the SSA of clay, the internal SSA should be considered, especially bentonite. Yukselen-Aksoy and Kaya [63] used the BET, EGME, MB test methods to determine the SSA of 32 soils with different mineralogies, but results showed a big difference by different methods. After

investigating 267 groups of samples, Deng et al. [64] also found that only when the SSA was about 80 m^2/g would there be a good relationship between the consistency limit and SSA. Hong et al. [11] found that even though the relationship was fitted by a large number of LL and SSA data, the predicted hydraulic conductivity still ranged between 1/3 and three times to the laboratory test value. Additionally, after checking more than 500 datasets from the literature, Spagnoli and Shimobe [65] found that even the relations of SSA with LL were robust, but the estimated SSA values slightly overestimated the measured SSA up to 100 m^2/g.

Above all, many definitions and methods have been given to determine the effective e and SSA of the soil, but there are significant differences between each method, especially for clay. At present, the effective e in undisturbed soil is more of a conceptual existence and there is still no clear and effective method to determine it. This is because most of the effective e is based on the e, but the current methods for determining e mainly include weighing after drying, compression tests, or by controlling the volume of solid during sample preparing in the laboratory. These methods either destroy the original structure of the clay samples or contain unconnected pores. Similarly, in the current methods of calculating the SSA of clay, the samples are mostly ground and dried into particles. So, the SSA measured by these methods are the SSA of soil particles. For clay, due to the influence of the adsorbed water and the double electric layer (DEL), water cannot flow over the surface of each particle, so there are many unconnected pores and small pores tend to have no contribution to seepage. Therefore, the e and SSA obtained by the current test methods cannot reflect the real characteristics of pore structure during clay seepage. These may be the reasons for which there is a large deviation of the original K-C equation in predicting the permeability of clay.

So, in this paper, the influence of mineralogy on pore micro-structure and permeability of clay and sandy soil are analyzed. Then, the conception of effective e (e_{eff}) and effective SSA (S_{eff}) are proposed by considering the influence of adsorbed water and unconnected pores under seepage state. Based on this, the permeability prediction model modified on K-C equation by e_{eff} and S_{eff} is proposed. In order to test the rationality of e_{eff}, S_{eff} and the applicability of this model to clay, S type of artificial clay samples with different porosity and Y type of natural clay samples with different natural clay content are designed for permeability tests. At the same time, the freeze-drying method and MIP test are used to obtain the e_{eff} and S_{eff}. Then the SSA, e and hydraulic conductivity by different method are compared, and the result showed that the prediction model proposed in this paper had an outstanding performance in predicting the hydraulic conductivity of clay. The research results of this paper have certain significance to solve the academic problem that K-C equation cannot be used in clay, and also are significant to ensure the safety of building foundation pits in clay areas.

2. Effective Pores and the Permeability Prediction Model Modified on K-C Equation

2.1. Effective Pores of Clay Seepage

Clay is mainly composed of clay minerals, such as montmorillonite, kaolinite and illite. These mineral crystals are mostly made up of silicon sheets, brucite sheets and gibbsite sheets. However, the bonds holding the unit layers together may be sufficiently weak and easily influenced by the environment, so isomorphous substitution in all the clay minerals gives clay particles a net negative charge [66]. The net negative charges adsorb cations and polar water molecules to form DEL (Figure 1). Some scholars referred to several layers of water molecules adsorbed on the surface of the particles as strongly adsorbed water and believe that strongly adsorbed water could not flow [41]. Affected by the crystal structure of clay minerals, the clay particles are mostly small flakes. During deposition, the flakes are stacked in various forms by the interaction between electric field forces, gravity and van der Waals forces. This random stack creates many types of pores inside the clay (Figure 2). Among them, some pores are self-locking and the water in the pores cannot flow, these are called isolated pores and blind pores. However, for some small pores such as the gaps of

the flakes, even though they are interconnected but the liquid still cannot flow through them due to the DEL and the adsorbed water [67]. Therefore, these small pores, the above isolated pores and blind pores are all invalid pores for clay seepage.

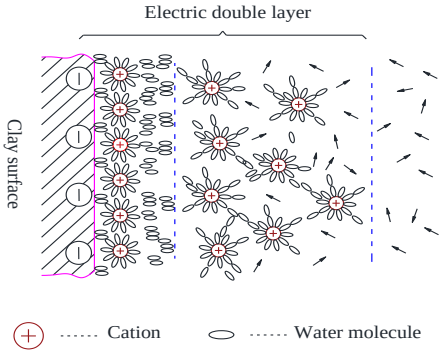

Figure 1. Schematic diagram of diffuse electric double layer.

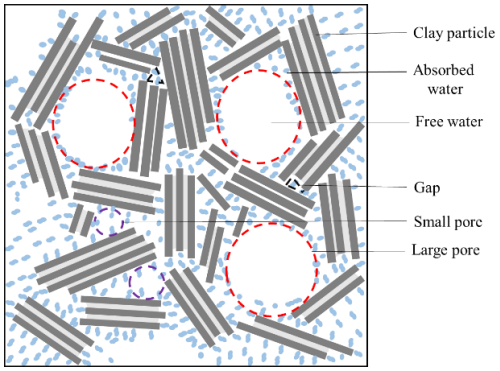

Figure 2. Pore structure of clay in microscope.

In fact, for sandy and silt soil, the particle size is large, and particles behave as independent units. This kind of independent particle mostly contacts by point-point, so the pores are mostly interconnected. Therefore, the fluid can be considered to flow through all the surface of particles. In this case, it is acceptable to use the surface area of the particles to represent the tube surface area in the K-C equation and obtain a closer result to the experiment. For clay, due to the combined effects of mineral crystal structure, clay particle shape, surface charge and adsorbed water, some pores are blind, isolated and unconnected, so the fluid in the clay shows an obvious difference from that in sandy and silt soil, as shown in Figure 3. When seepage occurs in clay, the fluid cannot flow over the surface of all particles but only flow over the surfaces of particles along the effective pores. In this case, there is a large gap between the flow area of the effective pores and the surface area of clay particles, so it is no longer reasonable to use the SSA of clay particles in the K-C equation.

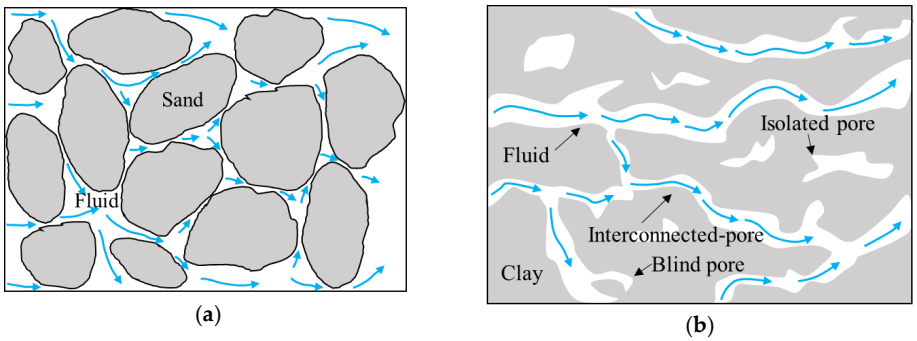

Figure 3. Internal seepage of different soils:(**a**) Sand and silty soil; (**b**) Clay.

2.2. The Permeability Prediction Model Modified on K-C Equation

For a capillary, by Poiseuille's law, the average flow velocity v_{ave} is shown as:

$$v_{ave} = \frac{\gamma_p R^2}{8\mu} i_h \tag{1}$$

where μ is the viscosity, R is the radius of the tube (Figure 4), γ_p is the specific gravity, and i_h is the hydraulic gradient. For a full-flow circular tube, the hydraulic radius is:

$$R_H = \frac{\pi R^2}{2\pi R} = \frac{R}{2} \tag{2}$$

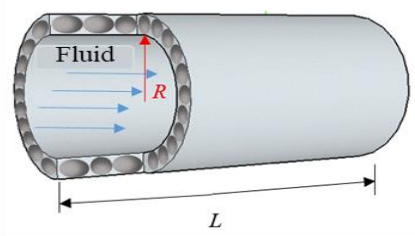

Figure 4. Tube model of soil seepage.

At this point, according to Poiseuille's formula, the fluid volume of the tube can be obtained as follows:

$$q_{cir} = \frac{\gamma_p R_H^2 i_h a}{2\mu} \tag{3}$$

where a is the cross-sectional area of the tube. For differently shaped pores, the shape factor C_s is introduced, then the former formula becomes as follows:

$$q_{cir} = C_s \frac{\gamma_p R_H^2 i_h a}{\mu} \tag{4}$$

For soils with a total cross-sectional area A, in the saturated state, the area of flow passages is A_f.

$$A_f = nA \tag{5}$$

where n is the porosity of the soil, and the hydraulic radius R_H can also be expressed as:

$$R_H = \frac{A_f}{P} = \frac{A_f L}{PL} = \frac{V_w}{V_s \rho_s S_p} \tag{6}$$

where P is the total circumference of the flow tubes, L is the length of the flow tube, V_w is the volume of the water and V_s is the volume of the solid, ρ_s is the density of soil particles. According to the introduction above, for clay, the fluid can only flow through interconnected pores, so S_p in this formula is the SSA of the pores, that is, the SSA of particles along the interconnected pores through which liquid can effectively flow. At this point, Equation (5) can be written as follows:

$$q = C_s \frac{\gamma_p}{\mu} \left(\frac{V_w}{V_s \rho_s S_p} \right)^2 i_h A_f \tag{7}$$

In this paper, except the unconnected pores, the absorbed water and the small pores that are influenced by absorbed water with no contribution to seepage are all treated as invalid, these parts are omitted when calculating the effective e [7,41]. The volume of adsorbed water is calculated according to the following formula:

$$V_{ab} = \delta \cdot S \tag{8}$$

where δ is the thickness of the adsorbed water and S is the SSA. If there are two or three layers of water molecules adsorbed on the particle surface, since the diameter of a single water molecule is 0.3 nm [41], then the effective radius of the tube becomes R − 0.6 nm or R − 0.9 nm. At the same time, according to the theory of Gouy-Chapman, the ion concentration of the soil in nature is between 0.83×10^{-2} mol/L and 0.83×10^{-4} mol/L [66]. The thicknesses of DEL are 3.33 nm and 33.3 nm (Figure 5), but not all liquids in the DEL cannot flow.

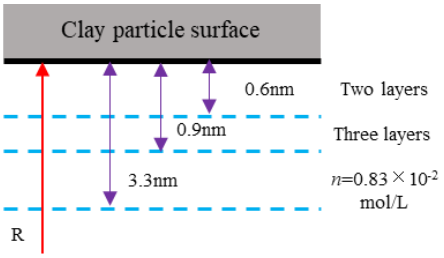

Figure 5. Influence of absorbed water or DEL.

Considering the above factors, in this paper, when the pore diameter is less than 3 nm, these pores are treated as invalid pores because they are influenced by absorbed water with no contribution to seepage. At this time, the volume of pores in the clay that have a positive contribution to the seepage can be expressed as:

$$V_v{}' = V_v - V_{ab} - V_{unc} - V_{noc} \tag{9}$$

where $V_v{}'$ is the effective pore volume, V_{noc} is the volume of pores influenced by absorbed water and with no contribution to seepage, V_{unc} is the volume of pores which are unconnected such as blind pores and isolated pores, these pores can be measured by MIP test. Then the effective e of the interconnected pores and shown as:

$$e_{\text{eff}} = \frac{V_v'}{V_s'} = \frac{V_v - V_{ab} - V_{unc} - V_{noc}}{V_s + V_{ab}} \tag{10}$$

where, V_s is the volume of soil particles, and $V_s{}'$ is the volume of soil particles plus the volume of adsorbed water. At this point, there is:

$$V_w = e_{\text{eff}} V_s' = e_{\text{eff}}(V_s + V_{ab}) \tag{11}$$

After subtracting the pores which have diameters less than 3 nm, the SSA of particles along the interconnected pores can be written as effective SSA (S_{eff}). Under stable laminar flow, substituting Equations (5), (10) and (11) into Equation (8), and changing the V_s to $V_s{}'$, the hydraulic conductivity is obtained according to Darcy's law:

$$k = C_s \frac{\gamma_p}{\mu} \left(\frac{e_{\text{eff}}(V_s + V_{ab})}{(V_s + V_{ab})\rho_s S_{\text{eff}}} \right)^2 \frac{e_{\text{eff}}}{1 + e_{\text{eff}}} = C_s \frac{\gamma_p}{\mu \rho_s^2 S_{\text{eff}}^2} \frac{e_{\text{eff}}^3}{(1 + e_{\text{eff}})} \tag{12}$$

In the formula, C_s is a coefficient describing the tortuosity of pores, and it is difficult to obtain the exact value. At present, this coefficient is mostly selected by experience. According to the works of Mitchell and Soga [66], in this model C_s is taken as 5. When S_{eff} and e_{eff} in the formula are taken as the specific surface area S and total pore e, the formula becomes the classic K-C equation.

3. Experimental Scheme and Result

3.1. Experimental Method and Scheme

(1) Experimental materials

The prediction model proposed in this paper is aimed at clay soil, so the experimental samples are all clay samples. Artificial soil mineral powder is often used to prepare soil samples in the laboratory because of its clear mineral composition and high purity. So, in this experiment, the artificial mineral powder of kaolinite and bentonite were used to prepare the S type samples. However, considering that the mineral composition of clay in nature is much more complex than that of artificial soil in the laboratory, and the permeability prediction model in this paper is eventually applied to the natural clay layer of the building foundation pit. So, the natural clay also was used to prepare the Y type soil samples in this experiment. The natural clay was selected from Nansha of Guangzhou, China, because there are thick soft clay layers distributed in this area. In order to ensure the samples selected from Nansha were clay soil, ten samples in the sampling area were sent for X-ray diffractometer test(Germany BRUKER D8 ADVANCE, Cu(monochrome)) and the test results are shown in Table 1.

Table 1. The mineral information for natural soil (Nansha, Guangzhou, China).

Sample No.	Quartz	Feldspar	Illite	Chlorite	Kaolinite	Others
N1	19.9		25.7	23.8	30.6	
N2	24.0	7.2	24.3	24.3	22.1	
N3	25.8		27.8	23.8	22.6	
N4	24.8		23.4	26.3	23.3	2.2
N5	21.4		16.9	30.0	31.8	
N6	22.5		26.3	24.4	26.9	
N7	24.0		24.9	19.9	29.3	1.9
N8	22.2		27.4	25.9	24.5	
N9	19.7		19.0	30.0	31.3	
N10	23.2		26.5	25.3	23.2	1.9

The results show that the clay mineral content of the natural soil in this area is very high, which can well meet the requirement.

(2) Experimental scheme

Void ratio and SSA are the key parameters to the K-C equation, which are also the starting points of the permeability prediction model proposed in this paper. Therefore, this test designed S type soil samples and Y type soil samples to test the applicability of this model to clay. For S type samples, by controlling the volume of solid particles, five groups of soil samples with different void ratios were designed. For Y type samples, the SSA of samples was controlled by adding a small amount of bentonite in natural soil. Therefore, six groups of soil samples with different bentonite content have been designed in Y type samples. The information of samples is shown in Table 2:

Table 2. The mixture table for the two types of soil samples.

No.	Component (m_{bent}:m_{kao})	Porosity	Test Items	No.	Component ($m_{natural}$:m_{bent})	Porosity	Test Items
S1	bentonite + kaolinite (0.134:1)	0.45	*PL*; I_P; *e*; SSA *k*	Y1	0.9:0.1	0.48	*PL*; I_P; *e*; SSA *k*
S2		0.5		Y2	0.85:0.15		
S3		0.55		Y3	0.8:0.2		
S4		0.6		Y4	0.75:0.25		
S5		0.65		Y5	0.7:0.3		
				Y6	0.65:0.35		

Among them, the proportion of bentonite and kaolin in S type samples and the porosity of Y type samples were determined according to relevant experience and literature [67]. After sample preparation, the liquid limit (LL) test, plastic limit (PL) test, hydraulic conductivity(*k*) test, SSA test by EGM, BET method and MIP test were conducted for each group of samples.

(3) Experimental method

The plasticity index and SSA (By EGME, BET method) test of the mixed clay sample. The powders of bentonite, kaolin and natural clay were dried and mixed evenly according to the proportion in Table 2 Then the SSA of the mixed powder were tested by EGME and BET methods. The testing process was strictly in accordance with the standard [68,69]. At the same time, after the mixed powder wetted overnight, the LL and PL of each sample were measured and then the plasticity index of each sample were calculated.

The seepage experimental test of the two type samples. The matrix materials were wetted and packaged overnight, and then moulded in samples with a diameter of 6.18 cm and a height of 4 cm according to the design requirements. Specimens were tested by a permeability test after being saturated by vacuum evacuation. Because the sample contains bentonite, it needs a long time to be saturated. In this test, the soil samples were soaked in water for 3 days after 3 h of vacuum evacuation. To ensure the soil sample was saturated during the experiment, the sample was loaded into the test equipment and saturated again by penetration saturation with the hydraulic gradient between 40 and 47.5. The experimental data were considered valid when all of the outlets had a significant amount of water flowing out through the samples and when penetration saturation proceeded to the 5th day [67,70]. As shown in Figure 6, the permeability experiment was the variable hydraulic gradient test, and the initial hydraulic gradient was 46.5. The hydraulic gradient was recorded again after two hours, and then repeated several times to calculate the hydraulic conductivity.

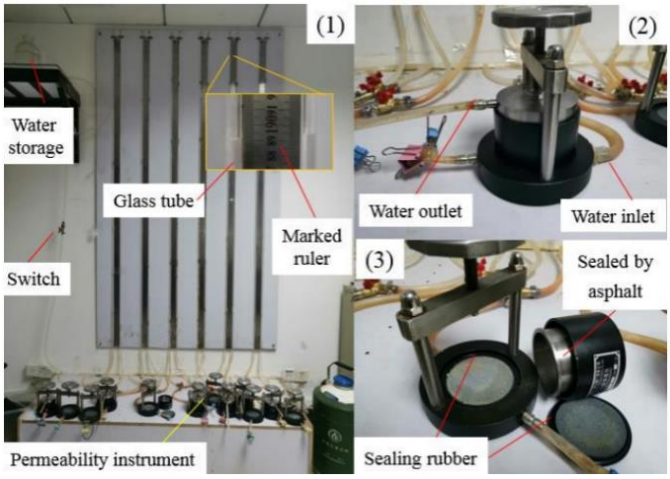

Figure 6. Permeability instruments: (1) Overall drawing of test equipment; (2) Permeameter; (3) Sealing method of specimen.

The MIP test for the void ratio and SSA of interconnected pores. After the hydraulic conductivity tests, the soil samples of each experimental point (such as S1) were cut out as 5 small samples with a volume of 1 cm × 1 cm × 1 cm. Then the small samples were quickly put into liquid nitrogen for freezing. After being frozen, these small samples were quickly placed in a freeze dryer and dried at −40 °C under vacuum [71,72]. The MIP test was carried out after the small samples were successfully prepared by freeze-drying method. The MIP test was carried out by the State Key Laboratory of Subtropical Architectural Science, China. The test instrument was AUTOPORE 9510 manufactured by Micromeritics company [73]. The relationship between pressure and the amount of Hg input was the MIP test, as shown in Figure 7.

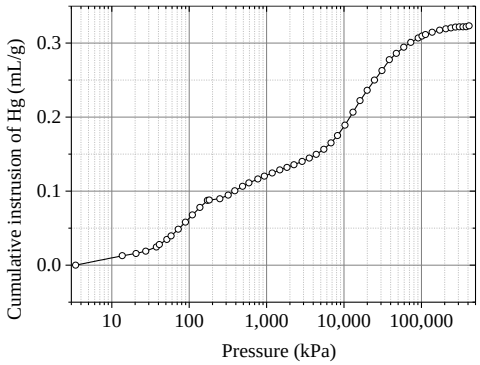

Figure 7. Curve of Cumulative volume of Hg with pressure.

The SSA of interconnected pores was obtained by the pressure and the volume of mercury injected:

$$S_p = \frac{1}{\sigma \cdot \cos\theta} \int_0^{V\max} p \cdot dV \tag{13}$$

where θ is the contact angle, p is the pressure value, σ is the surface tension of mercury, dV is the change in the volume of mercury injected, $V_{\max}$ is the maximum amount of mercury injected and S_p is the surface area of interconnected pores. In the MIP experiment, each sample was repeated three times to ensure the precision.

3.2. Experimental Results

(1) The SSA by different method

According to the experimental scheme and method, the SSA of two type samples measured by EGME, BET and the S_{eff} by MIP method are all shown in Table 3. At the same time, the SSA obtained by some classical estimated methods are also shown in the Table 3. The estimated methods are mainly proposed by scholars [7,63,74,75].

Table 3. SSA for two type soil by different method (m^2/g).

No.	*n*	Mass Ratio	EGME	BET	Smith et al. (1985) [74]	Churchman and Burke (1991) [75]	Yeliz Yukselen-Aksoy (2010) [63]	Ren (2016) [7]	S_{eff}
S1	0.45	0.143:1	79.8	19.8	411.1	45.7	135.9	106.0	13.0
S2	0.5	0.143:1	79. 8	19.8	411.1	45.7	135.9	106.0	12.5
S3	0.55	0.143:1	79. 8	19.8	411.1	45.7	135.9	106.0	12.4
S4	0.6	0.143:1	79. 8	19.8	411.1	45.7	135.9	106.0	12.2
S5	0.65	0.143:1	79. 8	19.8	411.1	45.7	135.9	106.0	12.2
Y1	0.48	0.1:1	108.2	26.1	388.2	41.7	124.1	100.2	21.5
Y2	0.48	0.15:1	124.1	27.1	431.0	49.1	132.9	111.0	21.8
Y3	0.48	0.2:1	138.7	21.4	470.3	55.9	140.9	121.0	22.0
Y4	0.48	0.25:1	152.1	28.0	506.4	62.1	148.4	130.2	22.9
Y5	0.48	0.3:1	164.5	29.5	539.8	67.8	155.2	138.6	23.6
Y6	0.48	0.35:1	175.9	30.2	570.7	73.1	161.6	146.5	24.4

The results in Table 3 show that among the results of the test methods, the SSA by the EGME method yielded the largest, the BET method was the second, and the MIP method was the smallest. For S type samples, the SSA by MIP test changes with the e, while the other methods are constant. For the Y type samples, the SSA of the samples changed obviously with the bentonite content by all methods. For the estimated methods, the SSA by Smith et al., Yeliz Yukselen-Aksoy, Ren and Churchman and Burke decrease by in order.

(2) The e_{eff} by different methods

When substituting the SSA (in Table 3) and the thickness of the adsorbed water layer into Equations (8)–(10), the e_{eff} is obtained and as shown in Figure 8.

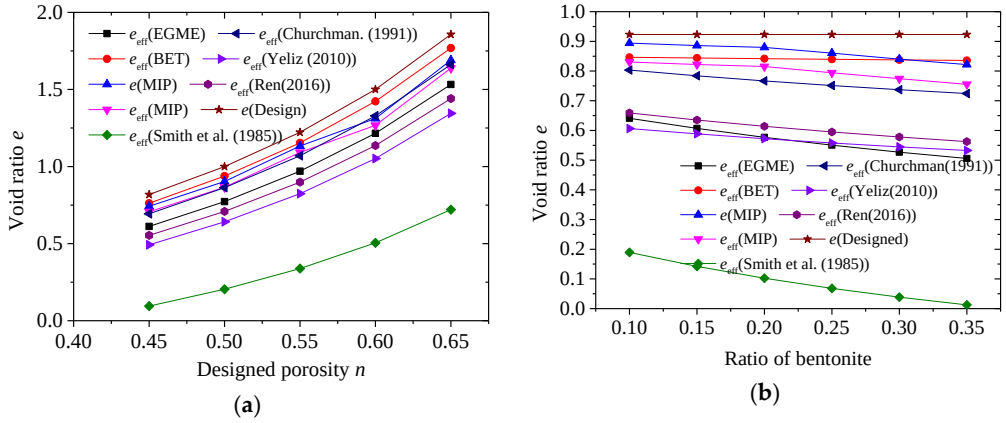

Figure 8. The e of two types soil samples: (**a**) S type soil samples; (**b**) Y type soil samples [7,63,74,75].

In Figure 8, for S type soil, the e_{eff} decreases with the decrease of the design porosity of the sample by all test methods. The e obtained by all test methods and estimated methods are smaller than the design e. Except the MIP method, the e_{eff} curves by other methods are almost parallel. For the Y type samples, the e_{eff} decreases with the increase of the bentonite content. Similarly, except the MIP method, the e_{eff} curves by other methods are almost parallel and linear.

(3) Hydraulic conductivity by different methods

When submitting the SSA and the corresponding e_{eff} obtained by various methods into Equation (12), the hydraulic conductivities can be obtained. In Figure 9, the hydraulic conductivities obtained by all methods increased with the increasing of e, and decreased with the increasing of bentonite content.

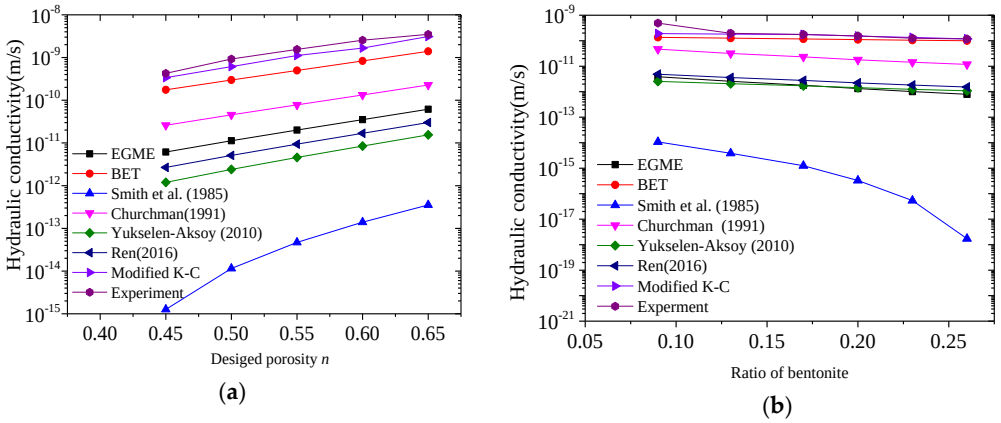

Figure 9. Hydraulic conductivities of two types of samples (**a**) S type samples; (**b**) Y type samples [7,63,74,75].

In Figure 9a, the results of the permeability prediction model modified K-C equation using S_{eff} and e_{eff} by MIP method achieves better agreement with the experimental values. The largest difference between them occurred when n = 0.5. At this point, the values of these two methods were 6.14 × 10^{-10} m/s (the modified model value) and 1.1 × 10^{-9} m/s (experimental values). The ratio of these two values was only 1.79, while the ratios for the other points were less than 1.6. For the BET and Churchman (1991) methods, the average ratios of the experimental values to the calculated values of the two methods were 3.1 and 19.85, while the other methods are 100 times larger, such as the method of Smith et al. (1985), and the ratio is astonishing at about 10,000 times. Similarly, for the Y type samples in Figure 9b, it could be seen that this modified equation still has advantages for natural remoulded soil. The results of this modified K-C equation by MIP method

and the experimental values at other points are coincident, except at the point when the bentonite ratio was 0.1. The average values of the experimental values to the calculated values of BET and Churchman are 1.73 and 8.5 respectively, and for the other methods, this value is much larger. At the same time, the hydraulic conductivity curves of the EGME, BET, Churchman, Yukselen-Aksoy and Ren clearly show almost linear changes, while the calculated values of MIP method are not linearly changed.

4. Discussion

4.1. The SSA and e_{eff} by Different Methods

There are two main reasons for the above phenomenon of SSA in Table 3. The first one is the special micro-structure induced by clay mineral property during seepage. Due to the influence of clay mineral properties, clay particles are mostly flake particles. There are negative charges on most clay mineral surfaces, and the negative charges always create electric forces between particles. Therefore, under the action of electric field forces, gravity and van der Waals forces, clay flakes more easily accumulate with each other to form a cluster structure. In cluster structure, there are many unconnected pores and tiny small pores. At the same time, the charges on the surface of clay particles also adsorb cations and polar water molecules to form DEL and adsorbed water. The DEL and adsorbed water often have a certain viscosity, and the adsorbed water is even considered to be immobile. So, the adsorbed water will occupy the effective pore of the clay. Except this, when the pores' size is very small, these pores are also considered as invalid pores because of the DEL and adsorbed water. Therefore, when the mineral composition or density of the sample changes, the internal micro-structure of the samples changes, so the e_{eff} and the S_{eff} change.

The second reason is that the SSA obtained by these test methods are different due to different test principles. Among these test methods, the EGME and BET method are aimed at particles; at the same time, the SSA by EGME is the total SSA of the particles, and the SSA by BET are the external SSA of the particles. So, in Table 3, the SSA for two types of samples by EGME method is larger than BET, because the total SSA is obviously bigger than external SSA. While for the estimated methods they are the empirical relationship between SSA and PL, I_p or SWCC, these methods are based on the EGME and BET tests. So, in Table 3 the SSA by Smith et al., Yeliz Yukselen-Aksoy and Ren methods are close to the values of EGME method, and the SSA by Churchman and Burke is close to the method of BET. However, for the MIP test, the test samples were prepared by the freeze-drying method, so the SSA by MIP test is the SSA of the interconnected pores of the seepage samples. That is to say, the MIP test aims at the clay with seepage structure while the EGME and BET test aim at the particle, which are essentially different. As mentioned above, clay particles are more easily to formed into a cluster structure. In this structure, particles that stack with each other will occupy the particle surface and the unconnected pores also reduce the SSA of the interconnected pores. So, the S_{eff} determined by MIP test is the smallest one.

In Table 3 the SSA of S type samples by EGME and BET method are constant, while the S_{eff} by MIP test increases with the designed porosity. This is because change of designed porosity cannot change the property of the particles, but can change the pore structure in the clay. Similarly, for Y type samples, even though the porosity is constant, the increase of bentonite content changes the surface properties of particles and the pore structure of the clay, so the SSA obtained by these methods all change with the bentonite content. Through the above discussion, it can be found that the S_{eff} obtained by MIP test method can simultaneously reflect the change of clay pore structure caused by the change of soil porosity, mineral composition and other factors.

These two reasons can also explain the phenomenon shown in Figure 9, since the e_{eff} is calculated by the SSA as show in Equation (11). The e_{eff} can reflect the influence of the adsorbed water, the disconnected pores and small pores on the effective pores for seepage. First, because there are invalid pores and the adsorbed water in clay, so the e_{eff} calculated by all methods are smaller than the designed e. Similarly, whether the mineral composition or the porosity of the sample changes, the amount of disconnected pores and small pores

all change, thus the e_{eff} is changed. At the same time, this can also explain why the soil e_{eff} curves in Figure 9, as except for the MIP method, the curves obtained by other methods are almost parallel and linear.

4.2. The Hydraulic Conductivity

The content in Figure 9can also be discussed from the test methods and the microstructure of the clay during seepage. As mentioned above, the total SSA by EGME and the external SSA by BET method are both aimed at the particles. However, the MIP method aims at the effective pores, so from Equations (11) and (12), the hydraulic conductivity calculated by S_{eff} is bigger than the SSA by EGME and BET methods. The estimated methods for SSA, such as Smith et al. (1985), Churchman (1991), Yukselen-Aksoy (2010) and Ren (2016) are all based on EGME and BET test. Since they are all empirical equations, the value of SSA calculated by some of them is too large; Therefore, the volume of adsorbed water calculated is amazingly big. So, the hydraulic conductivity calculated is too small and unreasonable.

Second, when the soil experiences seepage, the internal pore state is the decisive factor. For S type samples, within a certain range, when the density increases, the increase in the SSA of the pores indicates the increase in small pores. Under the influence of the adsorbed water and the DEL, the seepage efficiency of the small pores is very low, so the hydraulic conductivity decreases with the increase in the density (Figure 9a). For Y type samples, the expansion of bentonite makes it easier to form small pores, so the hydraulic conductivity of the soil decreases with the increase of the bentonite content. That is to say, the sample density and component are coupled to affect the connectivity of the pores, the S_{eff}, the e_{eff} and the hydraulic conductivity.

Unfortunately, the SSA used in the traditional calculation equations was mostly obtained by the EGME and BET test methods, while these two methods tested only the adsorption characteristics of minerals and could reflect only the basic properties of clay minerals. These two methods and the extended estimated methods could not reflect the pore connectivity of clay in a complex environment, so they could not reflect the real seepage situation of clay. The prediction model proposed in this paper by S_{eff} and e_{eff} considered the actual flow of the fluid in clay and used only the effective pore volume. Therefore, this prediction model had outstanding performance over the classic K-C equation. Additionally, it could achieve a high degree of concordance with the experimental values.

5. Conclusions

In the process of building pit construction, in order to solve the problem that the hydraulic conductivity of clay layer predicted by K-C equation always had a large deviation. In this paper, as showed in Figure A1, the properties of clay minerals and pore connectivity in clay were analyzed, then the permeability prediction model modified on K-C equation was proposed for clay by the S_{eff} and e_{eff}. In order to test the rationality of e_{eff}, S_{eff} and the applicability of this model to clay, seepage tests were conducted on two type of clay samples. At the same time, the freeze-drying method with MIP test were used to obtain the e_{eff} and S_{eff}. Then, the SSA, e and hydraulic conductivity by different methods were compared and discussed. Through the discussion, three main conclusions were obtained:

(1) The mineralogy of particles affects the internal pore structure of the clay and the behavior of liquids flowing over the particle surface. This is the fundamental reason why the seepage of clay is different from that of sandy soil. There are many pores invalid for seepage in clay, and the immobile adsorbed water also occupies the pore volume. Obviously, the SSA and e actually involved in seepage are overestimated in the classic K-C equation. It is the reason why the original K-C equation is biased in the seepage of clay.

(2) The e_{eff} and S_{eff} by the MIP method can better reflect the real pore structure of soil during the seepage process. The SSA obtained by EGME, BET and the estimated methods are the SSA of the particles. But the e_{eff} and S_{eff} are determined by the freeze-drying method

and MIP method, so the e_{eff} and S_{eff} aim at the effective pores in the clay during seepage. Therefore, e_{eff} and S_{eff} are influenced both by the clay density and composition.

(3) The permeability prediction model modified on K-C equation proposed in this paper is applicable to clay. This prediction model by the e_{eff} and S_{eff} show a good agreement with the experimental values. For S type, the largest difference between the prediction value and the experimental one is by the ratio of 1.79, while other points are less than 1.6. For Y type, except the point bentonite ratio which was 0.1, the results of the modified K-C equation and the experimental values at other points are almost coincident. In addition, through comparison, it is found that no matter what method is used to obtain e and S in the original K-C equation, the results of the seepage prediction model proposed in this paper are obviously outstanding. The research results of this paper have certain significance to solve the academic problem that the K-C equation cannot be used in clay and also are significant to ensure the safety of building foundation pits in clay areas.

Author Contributions: Conceptualization, J.C. and Y.F.; methodology, J.C.; resources, H.T.; data curation, R.G.; writing—original draft preparation, J.C.; writing—review and editing, J.Y.; supervision, Y.F.; funding acquisition, J.Y. All authors have read and agreed to the published version of the manuscript.

Funding: This research was funded by National Natural Science Foundation of China, the funder, Jie Yuan; the grant number, 51908151.

Data Availability Statement: The data presented in this study are available on request from the authors.

Conflicts of Interest: The authors declare no conflict of interest.

Appendix A

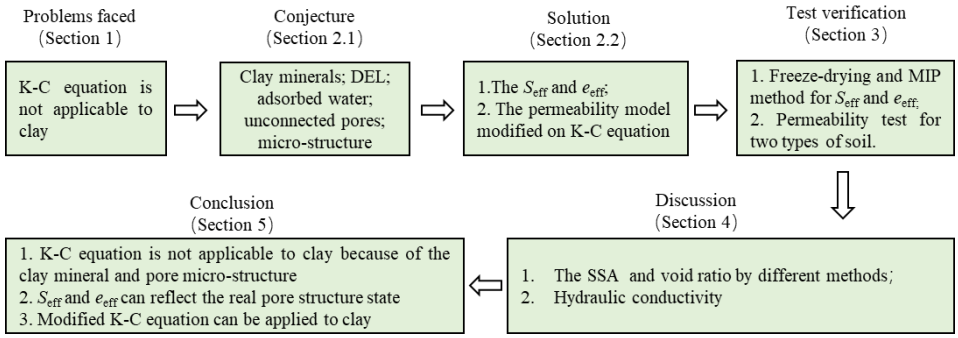

Figure A1. Research ideas of this paper.

References

1. Chang, W.; Wang, P.; Wang, H.; Chai, S.; Yu, Y.; Xu, S. Simulation of the Q(2) loess slope with seepage fissure failure and seismic response via discrete element method. *Bull. Eng. Geol. Environ.* **2021**, *80*, 3495–3511. [CrossRef]
2. Dong, H.; Huang, R.; Gao, Q. Rainfall infiltration performance and its relation to mesoscopic structural properties of a gravelly soil slope. *Eng. Geol.* **2017**, *230*, 1–10. [CrossRef]
3. Jie, Y.X.; Jie, G.; Mao, Z.; Li, G. Seepage analysis based on boundary-fitted coordinate transformation method. *Comput. Geotech.* **2004**, *31*, 279–283. [CrossRef]
4. Yao, Z.; Chen, Z.; Fang, X.; Wang, W.; Li, W.; Su, L. Elastoplastic damage seepage-consolidation coupled model of unsaturated undisturbed loess and its application. *Acta Geotech.* **2020**, *15*, 1637–1653. [CrossRef]
5. Ba-Phu, N.; Kim, Y. An analytical solution for consolidation of PVD-installed deposit considering nonlinear distribution of hydraulic conductivity and compressibility. *Eng. Comput.* **2019**, *36*, 707–730.
6. Pane, V.; Croce, P.; Znidarcic, D.; Ko, H.-Y.; Olsen, H.W.; Schiffman, R.L. Effects of consolidation on permeability measurements for soft clay. *Géotechnique* **1983**, *33*, 67–72. [CrossRef]
7. Ren, X.; Zhao, Y.; Deng, Q.; Kang, J.; Li, D.; Wang, D. A relation of hydraulic conductivity—Void ratio for soils based on Kozeny-carman equation. *Eng. Geol.* **2016**, *213*, 89–97. [CrossRef]
8. Chapuis, R.P. Predicting the saturated hydraulic conductivity of soils: A review. *Bull. Eng. Geol. Environ.* **2012**, *71*, 401–434. [CrossRef]

9. Zhang, F.; Wang, T.; Liu, F.; Peng, M.; Bate, B.; Wang, P. Hydro-mechanical coupled analysis of near-wellbore fines migration from unconsolidated reservoirs. *Acta Geotech.* **2022**, *17*, 3535–3551. [CrossRef]
10. Wang, M.; Wang, J.; Xu, G.; Zheng, Y.; Kang, X. Improved model for predicting the hydraulic conductivity of soils based on the Kozeny–Carman equation. *Hydrol. Res.* **2021**, *52*, 719–733. [CrossRef]
11. Hong, B.; Li, X.; Wang, L.; Li, L.; Xue, Q.; Meng, J. Using the effective void ratio and specific surface area in the Kozeny-Carman Equation to predict the hydraulic conductivity of loess. *Water* **2020**, *12*, 24. [CrossRef]
12. Jang, J.; Narsilio, G.A.; Santamarina, J.C. Hydraulic conductivity in spatially varying media—A pore-scale investigation. *Geophys. J. Int.* **2015**, *184*, 1167–1179. [CrossRef]
13. Chai, J.C.; Agung, P.M.A.; Hino, T.; Igaya, Y.; Carter, J.P. Estimating hydraulic conductivity from piezocone soundings. *Geotechnique* **2011**, *8*, 699–708. [CrossRef]
14. Costa, A. Permeability-porosity relationship: A reexamination of Kozeny-Carman equation based on a fractal pore-space geometry assumption. *Geophys. Res. Lett.* **2006**, *33*, 87–94. [CrossRef]
15. Asger, M.N.; Fridolin, O.; Henrik, B. Reexamination of Hagen-Poiseuille flow: Shape dependence of the hydraulic resistance in microchannels. *Phys. Rev. E* **2005**, *71*, 057301.
16. Chapuis, R.P.; Legare, P.P. A simple method for determining the surface area of fine aggregates and fillers in bituminous mixtures. In Proceedings of the Effects of Aggregates and Mineral Fillers on Asphalt Mixture Performance, San Diego, CA, USA, 10 December 1991; pp. 177–186.
17. Samarasinghe, A.M.; Huang, Y.H.; Drnevich, V.P. Permeability and consolidation of normally consolidated soils. *J. Geotech. Eng. Div.* **1982**, *108*, 835–850. [CrossRef]
18. Childs, E.C. Dynamics of fluids in Porous Media. *Eng. Geol.* **1972**, *7*, 174–175. [CrossRef]
19. Mesri, G.; Olson, R.E. Consolidation characteristics of montmorillonite. *Geotechnique* **1971**, *4*, 341–352. [CrossRef]
20. Taylor, D.W. Fundamentals of soil mechanics. *Soil Sci.* **1948**, *66*, 161. [CrossRef]
21. Carman, P.C. Permeability of saturated sands, soils and clays. *J. Agric. Sci.* **1939**, *2*, 12. [CrossRef]
22. Carman, P.C. Fluid flow through granular beds. *Chem. Eng. Res. Des.* **1937**, *75*, S32–S48. [CrossRef]
23. Kozeny, J. Uber Kapillare Leitung des Wassers im Boden. *Sitzungsber. Akad. Wiss.* **1927**, *136*, 271–306.
24. Li, M.; Chen, H.; Li, X.; Liu, L.; Lin, J. Permeability of granular media considering the effect of grain composition on tortuosity. *Int. J. Eng. Sci.* **2022**, *174*, 103658. [CrossRef]
25. Xu, P.; Zhang, L.; Rao, B.; Qiu, S.; Shen, Y.; Wang, M. A fractal scaling law between tortuosity and porosity in porous media. *Fractals* **2020**, *28*, 2050025. [CrossRef]
26. Xiao, B.; Wang, W.; Zhang, X.; Long, G.; Fan, J.; Chen, H.; Deng, L. A novel fractal solution for permeability and Kozeny-Carman constant of fibrous porous media made up of solid particles and porous fibers. *Powder Technol.* **2019**, *349*, 92–98. [CrossRef]
27. Bayesteh, H.; Mirghasemi, A.A. Numerical simulation of porosity and tortuosity effect on the permeability in clay: Microstructural approach. *Soils Found.* **2015**, *55*, 1158–1170. [CrossRef]
28. Luo, L.; Yu, B.; Cai, J.; Zeng, X. Numerical simulation of tortuosity for fluid flow in two-dimensional pore fractal models of porous media. *Fractals* **2014**, *22*, 1450015. [CrossRef]
29. Matyka, M.; Khalili, A.; Koza, Z. Tortuosity-porosity relation in porous media flow. *Phys. Rev. E* **2008**, *78*, 026306. [CrossRef]
30. Scholes, O.N.; Clayton, S.A.; Hoadley, A.F.A.; Tiu, C. Permeability anisotropy due to consolidation of compressible porous media. *Transp. Porous Media* **2007**, *68*, 365–387. [CrossRef]
31. Ichikawa, Y.; Kawamura, K.; Fujii, N.; Kitayama, K. Microstructure and micro/macro-diffusion behavior of tritium in bentonite. *Appl. Clay Sci.* **2004**, *26*, 75–90. [CrossRef]
32. Mathavan, G.N.; Viraraghavan, T. Coalescence/filtration of an oil-in-water emulsion in a peat bed. *Water Res.* **1992**, *26*, 91–98. [CrossRef]
33. Bear, J. *Dynamics of Fluids in Porous Media*; Elsevier: New York, NY, USA, 1972.
34. Ahuja, L.R.; Naney, J.W.; Williams, R.D. Estimating soil water characteristics from simpler properties or limited Data. *Soil Sci. Soc. Am. J.* **1985**, *49*, 1100–1105. [CrossRef]
35. Ahuja, L.R.; Naney, J.W.; Green, R.E.; Nielsen, D.R. Macroporosity to characterize spatial variability of hydraulic conductivity and effects of land management. *Soil Sci. Soc. Am. J.* **1984**, *48*, 699. [CrossRef]
36. Horton, R.; Thompson, M.L.; Mcbride, J.F. Estimating transit times of noninteracting pollutants through compacted soil materials. *Soil Sci. Soc. Am. J.* **1985**, *51*, 48–53. [CrossRef]
37. Meegoda, N.J.; Knodel, P.C.; Gunasekera, S.D. A new method to measure the effective porosity of clays. *ASTM Geotech. Test. J.* **1992**, *15*, 12.
38. Antognozzi, M.; Humphris, A.; Miles, M.J. Observation of molecular layering in a confined water film and study of the layers viscoelastic properties. *Appl. Phys. Lett.* **2001**, *78*, 300–302. [CrossRef]
39. Dolinar, B.; Trcek, B. A new relationship between the mobile and the adsorbed water in fine-grained soils using an effective void-ratio estimation. *Bull. Eng. Geol. Environ.* **2019**, *78*, 4623–4631. [CrossRef]
40. Koponen, A.; Kataja, M.; Timonen, J. Permeability and effective porosity of porous media. *Phys. Rev. E* **1997**, *3*, 3319–3325. [CrossRef]
41. Singh, P.N.; Wallender, W.W. Effects of adsorbed water layer in predicting saturated hydraulic conductivity for clays with Kozeny–Carman equation. *J. Geotech. Geoenvironmental Eng.* **2008**, *134*, 829–836. [CrossRef]

42. Urumović, K.; Urumović, S.K. The effective porosity and grain size relations in permeability functions. *Hydrol. Earth Syst. Sci. Discuss.* **2014**, *11*, 6675–6714.
43. Sanzeni, A.; Colleselli, F.; Grazioli, D. Specific surface and hydraulic conductivity of fine-grained soils. *J. Geotech. Geoenvironmental Eng.* **2013**, *139*, 1828–1832. [CrossRef]
44. Indraratna, B.; Trani, L. The use of particle size distribution by surface area method in predicting the saturated hydraulic conductivity of graded granular soils. *Géotechnique* **2010**, *60*, 957–962.
45. Carrier, W.D., III. Goodbye, Hazen; Hello, Kozeny-Carman. *J. Geotech. Geoenvironmental Eng.* **2003**, *129*, 1054–1056. [CrossRef]
46. Gregg, S.; Sing, K. *Adsorption Surface Area and Porosity*; Academic Press: London, UK, 1967.
47. Santamarina, J.C.; Klein, K.A.; Wang, Y.H.; Prencke, E. Specific surface: Determination and relevance. *Can. Geotech. J.* **2002**, *39*, 233–241. [CrossRef]
48. Phelps, G.W.; Harris, D.L. Specific surface and dry strength by methylene blue adsorption. *Ceram. Bull.* **1968**, *12*, 1146–1150.
49. Churchman, G.J.; Burke, C.M.; Parfitt, R.L. Comparison of various methods for the determination of specific surfaces of sub soils. *Eur. J. Soil Sci.* **2010**, *42*, 449–461. [CrossRef]
50. Cerato, A.B.; Lutenegger, A.J. Determination of surface area of fine-grained soils by the Ethylene Glycol Monoethyl Ether (EGME) method. *Geotech. Test. J.* **2002**, *25*, GTJ11087J.
51. Brunauer, S.; Emmett, P.H.; Teller, E. Adsorption of gases in multimolecular layers. *J. Am. Chem. Soc.* **1938**, *60*, 309–319. [CrossRef]
52. Garzón, E.; Sánchez-Soto, P.J. An improved method for determining the external specific surface area and the plasticity index of clayey samples based on a simplified method for non-swelling fine-grained soils. *Appl. Clay Sci.* **2015**, *115*, 97–107. [CrossRef]
53. Akin, I.D.; Likos, W. Single-point and multi-point water-sorption methods for specific surface areas of clay. *Geotech. Test. J.* **2016**, *39*, 20150117. [CrossRef]
54. Locat, J.; Lefebvre, G.; Ballivy, G. Mineralogy, chemistry, and physical properties interrelationships of some sensitive clays from Eastern Canada. *Can. Geotech. J.* **1984**, *21*, 530–540. [CrossRef]
55. Cerato, A. Influence of Specific Surface Area on Geotechnical Characteristics of Fine-Grained Soils. Master's Thesis, Civil Engineering, College of Engineering, University of Massachusetts, Amherst, MA, USA, 2001.
56. Macek, M.; Mauko, A.; Mladenovic, A.; Majes, B.; Petkovsek, A. A comparison of methods used to characterize the soil specific surface area of clays. *Appl. Clay Sci.* **2013**, *83–84*, 144–152. [CrossRef]
57. Kobayashi, I.; Owada, H.; Ishii, T.; Iizuka, A. Evaluation of specific surface area of bentonite-engineered barriers for Kozeny-Carman law. *Soils Found.* **2017**, *57*, 683–697. [CrossRef]
58. Ismeik, M.; Al-Rawi, O. Modeling soil specific surface area with artificial neural networks. *Geotech. Test. J.* **2021**, *37*, 20130146. [CrossRef]
59. Sharma, A.; Hazra, B.; Spagnoli, G.; Sekharan, S. Probabilistic estimation of specific surface area and cation exchange capacity: A global multivariate distribution. *Can. Geotech. J.* **2021**, *58*, 1077–1094. [CrossRef]
60. Meegoda, J.N.; Martin, L. In-situ determination of specific surface area of clays. *Geotech. Geol. Eng.* **2019**, *37*, 465–474. [CrossRef]
61. Dolinar, B. Predicting the hydraulic conductivity of saturated clays using plasticity-value correlations. *Appl. Clay Sci.* **2009**, *45*, 90–94. [CrossRef]
62. Dolinar, B.; Misic, M.; Trauner, L. Correlation between surface area and atterberg limits of fine-grained soils. *Clays Clay Miner.* **2007**, *55*, 519–523. [CrossRef]
63. Yukselen-Aksoy, Y.; Kaya, A. Method dependency of relationships between specific surface area and soil physicochemical properties. *Appl. Clay Sci.* **2010**, *50*, 182–190. [CrossRef]
64. Deng, Y.; Liu, Q.; Cui, Y.; Wang, Q.; Liu, S. Revisiting relationships among specific surface area, soil consistency limits, and group index of clays. *J. Test. Eval.* **2019**, *47*, 1392–1404. [CrossRef]
65. Spagnoli, G.; Shimobe, S. A statistical reappraisal of the relationship between liquid limit and specific surface area, cation exchange capacity and activity of clays. *J. Rock Mech. Geotech. Eng.* **2019**, *11*, 874–881. [CrossRef]
66. Mitchell, J.K.; Soga, K. *Fundamentals of Soil Behavior*, 3rd ed.; John Wiley & Sons: Hoboken, NJ, USA, 2005.
67. Chen, J.; Fang, Y.; Gu, R.; Shu, H.; Ba, L.; Li, W. Study on pore size effect of low permeability clay seepage. *Arab. J. Geosci.* **2019**, *12*, 238. [CrossRef]
68. *GB/T 50123-2019*; Standard for Geotechnical Testing Method. Ministry of Housing and Urban-Rural Development: Beijing, China, 2019.
69. *BS ISO 9277-2010*; Determination of the Specific Surface Area of Solids by Gas Adsorption. BET Method. BSI Group: London, UK, 2010.
70. *ASTM D2434-68(2000)*; Standard Test Method for Permeability of Granular Soils (Constant Head). ASTM: West Conshohocken, PA, USA, 2000.
71. Zeng, Z.; Cui, Y.J.; Talandier, J. Evaluating the influence of soil plasticity on hydraulic conductivity based on a general capillary model. *Eng. Geol.* **2020**, *278*, 105826. [CrossRef]
72. Wang, Q.; Cui, Y.-J.; Tang, A.M.; Li, X.-L.; Ye, W.-M. Time- and density-dependent microstructure features of compacted bentonite. *Soils Found.* **2014**, *54*, 657–666. [CrossRef]
73. Chen, B.; Zhang, H.; Chen, P. Influence of hyper-alkaline solution infiltration on microscopic pore structure of compacted GMZ bentonite. *J. Zhejiang Univ. Eng. Sci.* **2013**, *47*, 602–608.

74. Smith, C.W.; Hadas, A.; Dan, J.; Koyumdjisky, H. Shrinkage and Atterberg limits in relation to other properties of principal soil types in Israel. *Geoderma* **1985**, *35*, 47–65. [CrossRef]
75. Churchaman, G.J.; Burke, C.M. Properties of sub soils in relation to various measures of surface area and water content. *Eur. J. Soil Sci.* **1991**, *42*, 463–478. [CrossRef]